



ELSEVIER

Contents lists available at ScienceDirect

## Journal of Magnetism and Magnetic Materials

journal homepage: [www.elsevier.com/locate/jmmm](http://www.elsevier.com/locate/jmmm)

# Nondimensional scaling of magnetorheological rotary shear mode devices using the Mason number



Andrew C. Becnel, Stephen Sherman, Wei Hu, Norman M. Wereley<sup>\*,1</sup>

Department of Aerospace Engineering, University of Maryland, College Park, MD 20742 USA

## ARTICLE INFO

### Article history:

Received 26 June 2014

Received in revised form

10 October 2014

Accepted 13 October 2014

Available online 22 October 2014

### Keywords:

Magnetorheological fluids

Shear mode

Rotary energy absorbers

Shear rate

Mason number

Bingham plastic

## ABSTRACT

Magnetorheological fluids (MRFs) exhibit rapidly adjustable viscosity in the presence of a magnetic field, and are increasingly used in adaptive shock absorbers for high speed impacts, corresponding to high fluid shear rates. However, the MRF properties are typically measured at very low ( $\dot{\gamma} < 1000 \text{ s}^{-1}$ ) shear rates due to limited commercial rheometer capabilities. A custom high shear rate ( $\dot{\gamma} > 10,000 \text{ s}^{-1}$ ) Searle cell magnetorheometer, along with a full scale rotary-vane magnetorheological energy absorber ( $\dot{\gamma} > 25,000 \text{ s}^{-1}$ ) are employed to analyze MRF property scaling across shear rates using a nondimensional Mason number to generate an MRF master curve. Incorporating a Reynolds temperature correction factor, data from both experiments is shown to collapse to a single master curve, supporting the use of Mason number to correlate low- and high-shear rate characterization data.

© 2014 Elsevier B.V. All rights reserved.

## 1. Introduction

Magnetorheological energy absorbers (MREAs) have been successfully implemented in semiactive crashworthy systems to protect occupants against impact, shock and blastloads, especially to protect the lumbar region of the human spine [1–3]. Shear rates in these MREAs typically range up to  $25,000 \text{ s}^{-1}$  or higher. However, data from low shear rate (up to  $1000 \text{ s}^{-1}$ ) characterization tests are typically extrapolated up to these high shear rates because of the dearth of high shear rate data. Both MR yield stress and fluid viscosity have been shown to vary with temperature [4,5]. Furthermore, MRFs are highly shear thinning materials, so they exhibit a significant reduction in viscosity as shear rate increases [6]. For these reasons, a wide variety of fluid characterization tests, which vary temperature, shear rate, and applied magnetic field are currently required to adequately determine the performance of a given MR fluid utilized in certain devices and environments, and consequently, predictive models such as the Herschel–Bulkley (HB) constitutive model typically employed to characterize measured rheological behavior must rely on a huge data set of characterization tests to be useful across the entire range of expected operating conditions. It is desirable therefore to reduce the overall amount of data required for determination of

the MR fluid behavior, while maintaining the ability to accurately predict any off-nominal change in performance.

The objective of this study is to use a nondimensional Mason number incorporating temperature dependent parameters to scale fluid performance data between a custom Searle-type magnetorheometer, capable of high quality test measurements at shear rates up to  $10,000 \text{ s}^{-1}$ , and a practical shear mode rotary vane magnetorheological energy absorber (RVMREA), which operates at shear rates over  $25,000 \text{ s}^{-1}$ , to assess the performance of a commercially available magnetorheological fluid (LORD Corporation MRF-140CG) over this range of shear rates. Thus, a limited set of test data is shown to provide enough information for the critical design of RVMREAs operating over this shear rate range ( $0\text{--}25,000 \text{ s}^{-1}$ ).

### 1.1. Magnetorheological fluid

A magnetorheological fluid (MRF) consists of magnetizable particles suspended in a nonmagnetizable carrier fluid. Commercially available MRFs use carbonyl iron spheres on the order of  $1\text{--}10 \mu\text{m}$  in diameter as the magnetizable particles, either a silicon- or hydrocarbon-based oil as the carrier fluid, and various additives to improve stability and settling rate.

In the absence of an applied magnetic field, the particles are randomly dispersed and will move with the fluid as it flows. When exposed to a magnetic field, the particles form chains parallel to the magnetic field lines and the MRF “solidifies.” These two

\* Corresponding author.

E-mail address: [wereley@umd.edu](mailto:wereley@umd.edu) (N.M. Wereley).

<sup>1</sup> Digital Object Identifier inserted by IEEE.

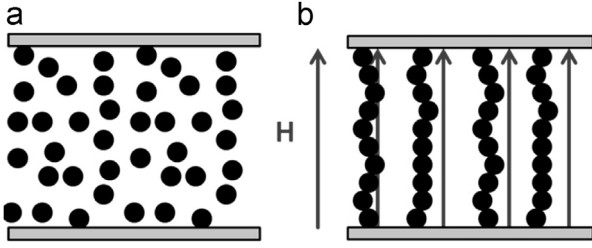


**Fig. 1.** States of magnetorheological fluid: (a) in the absence of field, the particles flow freely, (b) particles form chains that resist flow in the presence of magnetic field.

conditions of MRF, called “passive” and “active” respectively, can be seen in Fig. 1. The particle chains resist fluid motion until a certain yield stress is reached, beyond which fluid motion will occur, called post-yield flow [7].

In practical MRF devices, the magnetic field is produced by a controllable electromagnet. In this way the applied magnetic field, and thus the yield stress, can be continuously and instantaneously adjusted (response time < 15 ms), so that an appropriate amount of energy can be dissipated within the MREA. A well-developed MRF used in production devices will have a yield stress from 30 to 100 kPa at magnetic saturation.

## 1.2. Mason number and apparent viscosity

Classic work by Mason and colleagues showed that a non-dimensionalized ratio of dominating physical forces described particle behavior in shear and electric fields, and influenced following researchers to use a similar ratio [8]. This dimensionless group came to be known as the Mason number. A minimized expression for a Mason number is shown below as the ratio of hydrodynamic force to polarization force.

$$Mn \equiv \frac{F^H}{F_0} = \frac{\text{hydrodynamic}}{\text{polarization}} \quad (1)$$

Building on this framework, a Mason number for MRFs was developed based on the fluid shear rate and suspension magnetization [9]. Because the magnetization,  $M$ , is a nonlinear function of magnetic field strength within each particle, an appropriate polarization force term was a function of particle magnetization [10].

While the research by Klingenberg et al. [9] applied the same expression as for the hydrodynamic force as the original work, given as

$$F^H = 6\pi\eta_c a^2 \dot{\gamma} \quad (2)$$

where  $\eta_c$  is the carrier fluid viscosity,  $a$  is the particle radius, and  $\dot{\gamma}$  is the shear strain rate, they calculate the polarization force term as a modified point-dipole which accounts for nonlinearities in particle magnetization,  $M_p$ . Realizing that the magnetic moment is related to the average magnetization of a single spherical particle,  $m$ , by

$$m = \frac{\pi}{6} \sigma^3 M_p \quad (3)$$

where  $\sigma$  is the particle diameter, and that the bulk suspension magnetization,  $\langle M \rangle$  is related to the particle magnetization by the solids loading fraction,  $\phi$ , given by the equation

$$M_p = \frac{1}{\phi} \langle M \rangle \quad (4)$$

Klingenberg et al. [9] derive the magnetic polarization force to be the expression shown below:

$$F_0 = \frac{\pi \mu_0 \sigma^2 \langle M \rangle^2}{48 \phi^2} \quad (5)$$

where  $\mu_0$  is the permeability of free space,  $4\pi \times 10^{-7}$  [V s/A m].

An expression for Mason number in an MRF is given as

$$Mn(\dot{\gamma}, M) = \frac{9 \eta_c \phi^2 \dot{\gamma}}{2 \mu_0 \mu_c \langle M \rangle^2} \quad (6)$$

where  $\mu_c$  is the carrier fluid permeability. The Mason number given by Eq. (6) reduces the abscissa of the experimental characterization plots to a nondimensional expression, but in order to achieve the data collapse to a master curve it is helpful to also non-dimensionalize the ordinate. An accepted way to do this is to use apparent viscosity, the ratio of total shear stress by shear rate, and normalize this value by the high shear rate viscosity in the absence of applied field, as shown in the following equation:

$$\hat{\eta} = \eta_{app} / \eta_{\infty} \quad (7)$$

When experimental measurements of MR fluid apparent viscosity are plotted versus Mason number, the curves for various shear rates and magnetic field strengths collapse to a single function. Originally validated using low shear rate ( $\dot{\gamma} < 1000 \text{ s}^{-1}$ ) measurements, it was later shown to hold true in high shear rate operation [6] in carefully controlled laboratory experiments. It is proposed here that this nondimensional analysis can be effectively extended to model practical MREA devices under real-world conditions.

The experimentally measured variables are the shear rate,  $\dot{\gamma}$ , torque,  $M$ , and suspension magnetization,  $\langle M \rangle$ , and using this nondimensional group allows for disparate experimental data to be modeled as a single curve, greatly expanding the useable information about MR fluid behavior over a wide range of operating conditions.

It is worth mentioning that there are a number of other Mason numbers modified to account for surface friction and flow channel topography [11], suspensions of magnetizable particles in non-conducting media versus nonconducting particles in ferromagnetic media [12], and particle sizes in inverse ferrofluids [13]. Another study points out that there is an inconsistency in the choice of the characteristic particle dimension in Klingenberg's Mason number, specifically the use of particle radius,  $a$ , in the hydrodynamic force term of Eq. (2) and particle diameter,  $\sigma$ , in the magnetostatic force term of Eq. (3). The adjusted Mason number,  $Mn^*$ , would therefore be  $Mn^* = 32 \cdot Mn$  [14]. This definition of Mason number is used for the remainder of this study.

The rotary vane MREA is designed as a crash protection device, so it is expected to operate at high shear rates ( $\dot{\gamma} \geq 25,000 \text{ s}^{-1}$ ), approximately  $25 \times$  greater than can be achieved on commercial rheometers. We replace dynamic viscosity with the apparent viscosity,  $\eta_{app}$ , defined as the instantaneous ratio of the shear stress to the shear rate, and write the two term Bingham plastic model as shown below:

$$\eta_{app} = \frac{\tau_y}{\dot{\gamma}} + \mu \quad (8)$$

This requirement of using normalized apparent viscosity is because an MRF with a higher solids loading will be stronger due to a higher available yield stress, but the off state viscosity will also be larger. Therefore, a direct comparison across solids loading can be achieved by such a normalization. By relating the bulk suspension magnetization to the polarizing force through volume fraction in Eqs. (3) and (4), the Mason number implicitly accounts

**Table 1**  
Thermal scaling factor for viscosity–temperature relationship.

Fluid	$\beta$
MR132-DG, $\eta_0 = 0.092$	0.0664
MR140-CG, $\eta_0 = 0.21$	0.0653

for the fact that the same applied magnetic field will result in different, solids loading-dependent polarizing force.

### 1.3. Temperature correction factor

A typical hydrocarbon-based MR fluid has a viscosity that is related to its temperature through the relation given below [5,15]:

$$\eta = \eta_0 e^{\beta\phi(T-T_0)} \quad (9)$$

Using this relationship, a temperature-dependent Mason number can be defined from Eqs. (6) and (9) as

$$Mn(\dot{\gamma}, M, T) \equiv 144 \frac{\eta_c e^{-\beta\phi(T-T_0)} \phi^2}{\mu_0 \mu_c} \frac{\dot{\gamma}}{\langle M \rangle^2} \quad (10)$$

where the carrier fluid viscosity,  $\eta_c$ , is measured at reference temperature,  $T_0$ . The  $\beta$ -coefficients for 32 vol% and 40 vol% fluids are both approximately 0.066, given in Table 1.

## 2. Experimental setup

A common method to measure the behavior of an MRF is to use two concentric co-rotating cylinders, or Couette geometry, to impart a known angular velocity on the fluid while applying a variable magnetic field and measuring the torque produced. The relationship between these two measurements, known as flow curves, are the hallmark of rheometric studies and provide practical characterizations of fluid behavior. This is the same mode of operation used in the RVMREA, so an inner rotating cylinder (bob), combined with a fixed outer cylinder (cup), known collectively as a Searle cell, was chosen as the most appropriate magnetorheometer configuration [16].

### 2.1. Searle cell magnetorheometer

For this custom Searle cell magnetorheometer, torque–shear stress and rotation speed–shear rate relationships can be obtained from specifications for the cell geometry, schematically shown in Fig. 2.

These relationships are given in [17] and shown as follows. Shear stress,  $\tau$ , is given as

$$\tau = \frac{M}{2\pi L_c (R+h)^2} \quad (11)$$

where  $M$  is the measured torque. For the high shear rate magnetorheometer used in this research, the specific geometric parameters are listed Table 2.

An expression for the shear rate is obtained using cylindrical coordinates  $(\hat{r}, \hat{\theta}, \hat{z})$ , and noting that the 3D velocity vector field can be simplified to just a scalar,  $v_\theta$ , by assuming that the inner bob is sufficiently long in the axial direction relative to the gap size, such that  $v_z=0$ , and ensuring that the bob rotates at a constant angular velocity, such that  $v_r=0$ .

For narrow gaps, it can be assumed that the fluid is fully sheared in the  $\hat{\theta}$ -direction with the gradient in the  $\hat{r}$ -direction (the

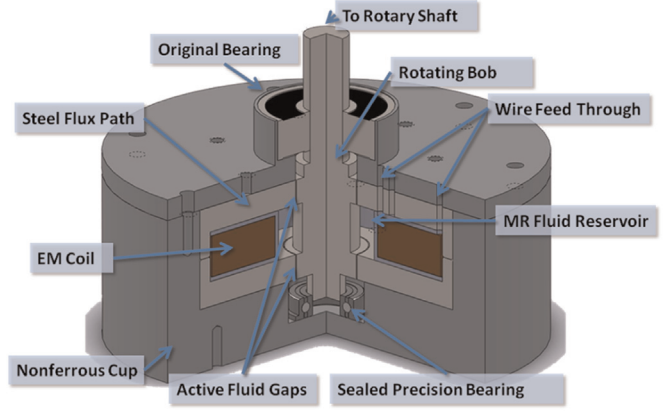


**Fig. 2.** Quarter-section of the Searle magnetorheometer cell.

**Table 2**  
Searle cell magnetorheometer dimensions.

	Measurement
<b>Searle cell parameter</b>	
Active gap length, $L_c$	12.0 mm
Bob radius, $R$	8.75 mm
Cup radius	9.0 mm
Active gap height, $h$	0.25 mm
Active fluid volume	2.36 mm <sup>3</sup>
<b>RVMREA parameter</b>	
Vane active length, $L_v$	74.2 mm
Vane mean radius, $R_{v,avg}$	49.5 mm
Vane thickness	5.1 mm
Bobbin, cylinder radii	46.55, 52.55 mm
Active gap heights $h_i, h_o$	0.4, 0.5 mm
Active fluid volume	95.6 mm <sup>3</sup>

velocity profile is linear in  $\hat{r}$ ) as shown below [18]:

$$v_\theta = C_1 r + C_2 \quad (12)$$

The constants  $C_1$  and  $C_2$  can be found using the boundary conditions for the Searle cell design, namely that of stationary cup,  $v_\theta = 0$  at  $r = R + h$ , and a rotating bob,  $v_\theta = R\omega_i$  at  $r = R$ . This yields

$$v_\theta = \frac{R(R+h-r)}{h} \omega_i \quad (13)$$

The rate-of-deformation tensor is sparse and can therefore be calculated as merely the derivative of Eq. (13) with respect to  $r$ , which greatly simplifies the issue of shear rate estimation and results in the narrow-gap shear rate expression [16] given below:

$$\dot{\gamma} = \frac{R}{h} \frac{2\pi}{60} \Omega \quad (14)$$

Control and data acquisition in the magnetorheometer are accomplished through the graphical programming software *LabVIEW* by National Instruments [19]. To generate the desired input rotation speed, a 0.75 HP (560 W) electric servomotor, model SilverMax 34-HC1 by QuickSilver Controls, Inc., is connected through a QCI CLCF-01 motor controller which receives voltage commands from the desktop PC running *LabVIEW*. This servomotor is capable of a maximum of 3000 rpm at 100 oz in (0.706 N m) of torque, ensuring that the commanded voltage results in a reliable motor speed [20]. This performance was also verified using an optical tachometer to measure the speed of rotation at a given voltage, which confirmed the input accuracy.

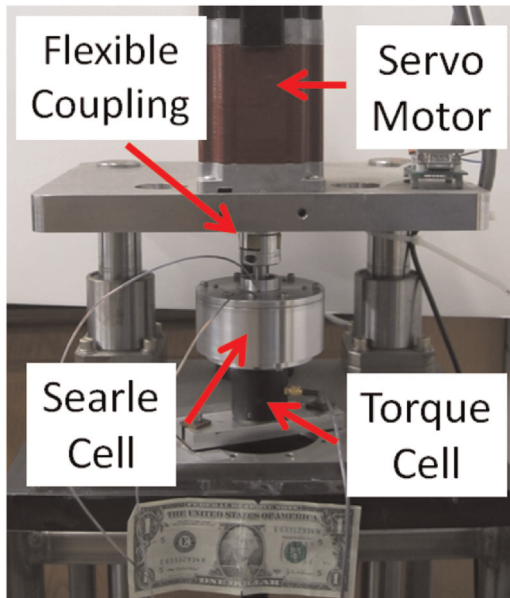


Fig. 3. Searle cell magnetorheometer.

The torque output is measured by a 100 ounce-inch (0.706 N m) torque transducer, model RTS-100, and the voltage signal is passed through a TM-02 signal conditioner, both by Transducer Techniques, which interfaces with the PC through a National Instruments BNC-2110 data acquisition box. The test setup is shown in Fig. 3.

The control and data acquisition program produces a staircase voltage signal, a waveform consisting of a series of discrete steps, shown in Fig. 4. This provides eight quasi-steady shear rate levels and allows for any transient effects to diminish following the speed changes. The user controls the maximum desired rotation speed, and the program divides this maximum into equally spaced steps, commands the servomotor, and outputs torque and temperature data.

In addition to plots of motor RPM and torque output, the magnetorheometer Searle cell was fit with a custom cooling jacket

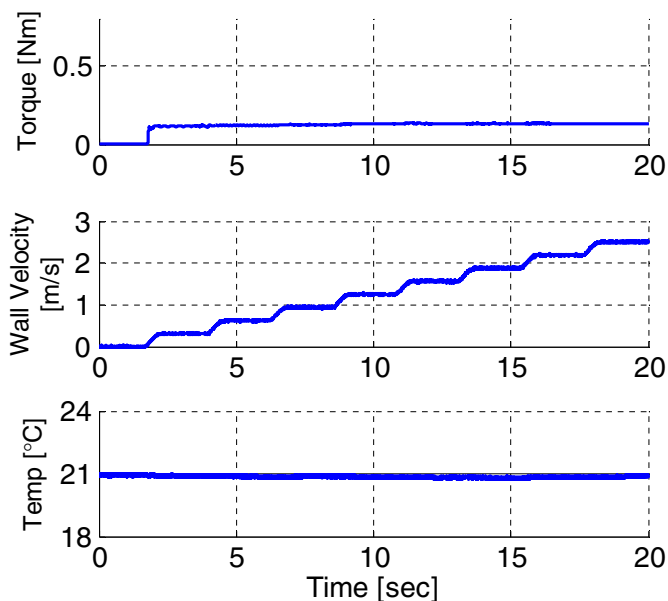


Fig. 4. Raw Searle cell magnetorheometer data for applied current of 0.5 A.

made from 12 turns of 0.25 in. copper tubing and an internal K-type thermocouple. The cooling jacket is connected to a circulator pump with thermostat-controlled refrigerating and heating capability, Julabo model F25-MD, allowing precise control over the internal fluid sample temperature. The internal thermocouple is inserted through the top cap of the magnetorheometer and rests within the central fluid chamber, without passing through the active gap region to avoid interfering with the flow.

The cooling jacket is a nonintrusive feature which allowed for isothermal tests to be performed. Using the cooling jacket to bring the entire MR cell to a steady temperature prior to starting an experiment, it is therefore possible to maintain a near constant temperature in the fluid sample while gathering rheometric data during the 21 s tests.

## 2.2. Rotary vane MREA

The RVMREA was designed such that the MRF is directly sheared in the presence of magnetic field within two “active gaps”. Its configuration, shown in Fig. 5, uses a thin cylindrical vane, attached to a shaft, which rotates between a stationary coil housing and body cylinder, so that the fluid is sheared within the MR fluid gaps. The magnetic field is supplied using an electromagnet, so the yield stress can be continuously, reversibly, and rapidly adjusted [15].

To evaluate the performance of the rotary vane MREA, a high speed transmission test rig (US Drives, Inc. Phoenix AC drive, connected to a Vector 75 HP drive motor) was used for torque measurements at speeds corresponding to low crash velocities. The complete test setup is shown in Fig. 6. The MREA was mounted on a stationary frame, while the rotary shaft of the MREA was connected to a DC motor via two flexible couplings and a torque sensor. A non-contact laser tachometer measured rotational speed, and a thermocouple was fixed to the outer surface of the RVMREA cylinder to monitor RVMREA temperature variation during testing (not shown in Fig. 6).

The DC motor provides a rotational speed of up to 1800 rpm, which translates into a velocity of approximately 2.5 m/s (8 ft/s) with a 1 in. diameter shaft,  $R_s = 1$  in. A BKPrecision XLN10014 DC power supply was used to supply constant current to the RVMREA during testing.

During the initial round of characterization tests, the nominal currents supplied were 0, 1.5 and 3.5 A. For each applied current,

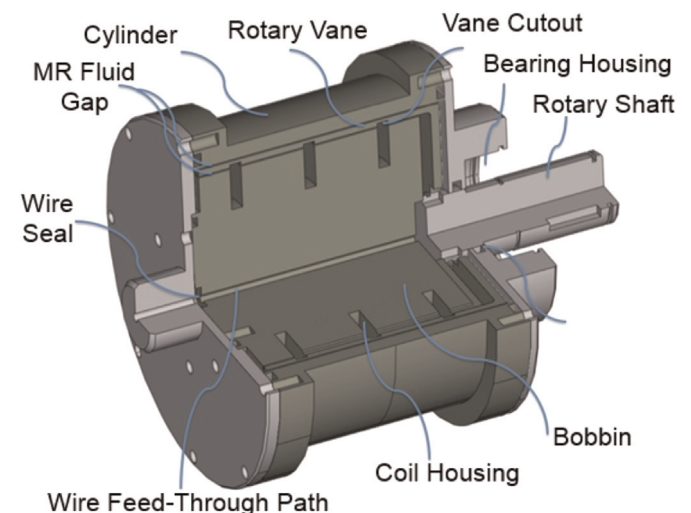


Fig. 5. Quarter section of RVMREA.

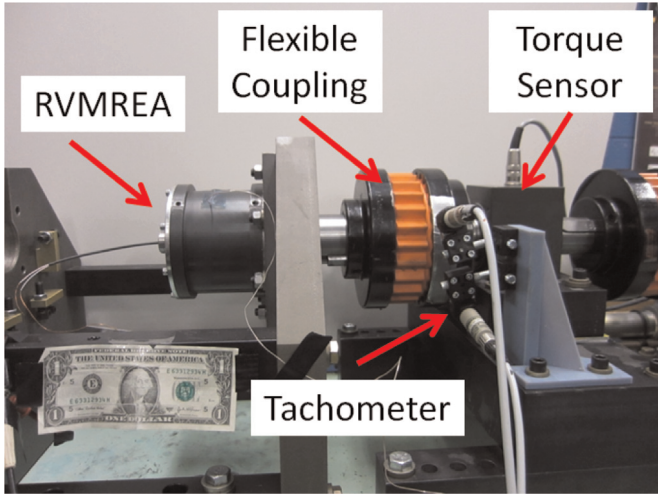


Fig. 6. Rotary vane MREA and test setup.

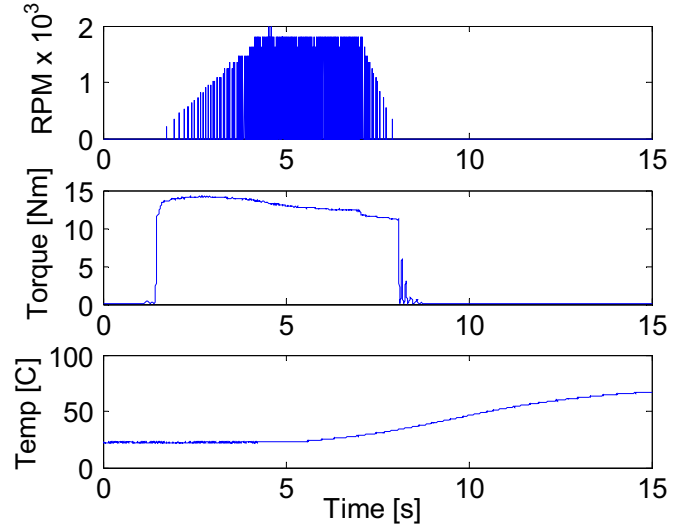


Fig. 7. Raw RVMREA experiment data for 3.5 A applied current.

the rotational speed for testing was increased from 0 rpm to 1800 rpm within 3 s and held at 1800 rpm for 2 s.

The relationship between torque output and total MR fluid shear stress within the RVMREA can be obtained through a modified version of Eq. (11), where the Searle cup inner radius ( $R + h$ ) has been replaced with an expression reflecting the new shear surface radii. The equation below reflects the fact that, in the case of the multiple shear gaps of the RVMREA (between the coil armature and the inner vane surface, referred to as the “inner gap”, and between the outer vane surface and the cylinder damper body, referred to as the “outer gap”), the total fluid shear stress can be amplified by using more shear surfaces, or vanes.

$$\tau = \frac{M}{2\pi L_v (R_a^2 + R_o^2)} \quad (15)$$

Here,  $L_v$  is the vane length,  $R_a$  is the coil armature outer radius and  $R_o$  is the inside radius of the cylinder damper body. For the inner gap, the shear stress expression contains only the  $R_a$  term; similarly, the outer gap shear stress expression contains only the  $R_o$  term. The relevant dimensions of the RVMREA are given in Table 2. The fluid shear rate within each narrow gap as a function of rotation rate in rpm,  $\Omega$ , is given as the following set of equations [18]:

$$\dot{\gamma}_i = \frac{R_{v,i}}{h_i} \frac{2\pi}{60} \Omega \quad (16)$$

$$\dot{\gamma}_o = \frac{R_{v,o}}{h_o} \frac{2\pi}{60} \Omega \quad (17)$$

The commercially available MRF selected for the scaling study is LORD Corporation’s MRF-140CG, containing 40 vol% of Fe particles. Each characterization was performed using a velocity profile incorporating a 2 s ramp and 3 s hold at 1800 rpm. In between tests the sample was allowed to return to ambient temperature (25 °C), resting for approximately 15 min between consecutive test runs. The RVMREA was then magnetized above the level used during the previous test to mitigate any remnant magnetization effects. A typical data set (Fig. 7) collected the commanded rotation input, the responding measured torque output, and the temperature.

### 3. Results

#### 3.1. Flow curves

Force versus velocity plots can be converted from torque and rotation speed for both the Searle magnetorheometer using Eqs. (11) and (14), and for the RVMREA using Eqs. (15) and (16), respectively. These tests generated flow curves across a range of applied magnetic field strengths, and results are shown in Figs. 8 and 9. Note that the largest current applied to the RVMREA, 3.5 A, corresponds to a magnetic field strength around 150 kA/m, resulting in the “saturation” – or maximum attainable yield stress – of the MRF. However, the correlation between applied current and shear stress differs between the smaller Searle cell magnetorheometer and the larger RVMREA, an issue that can be addressed by using the Mason number analysis presented later.

#### 3.2. Temperature corrected Mason number

As shown in Fig. 10, without a temperature-corrected Mason number, the characterization data fail to collapse to the expected master curve because of the substantial effect temperature has on

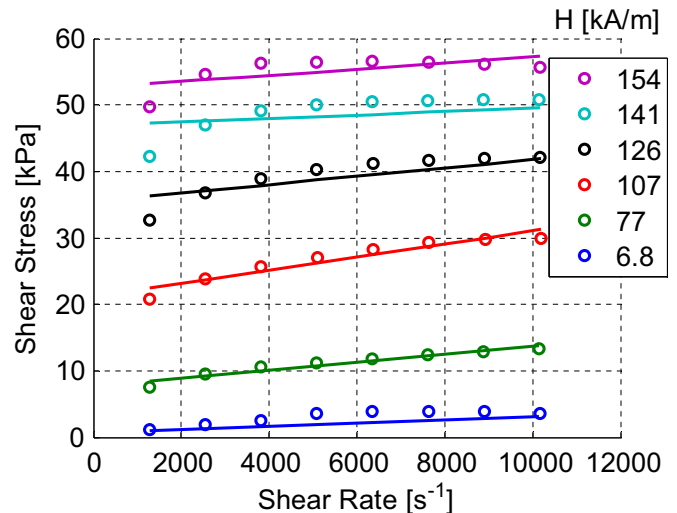


Fig. 8. Shear stress as a function of shear rate and applied field for MRF-140CG from the Searle magnetorheometer, with Bingham plastic fit.

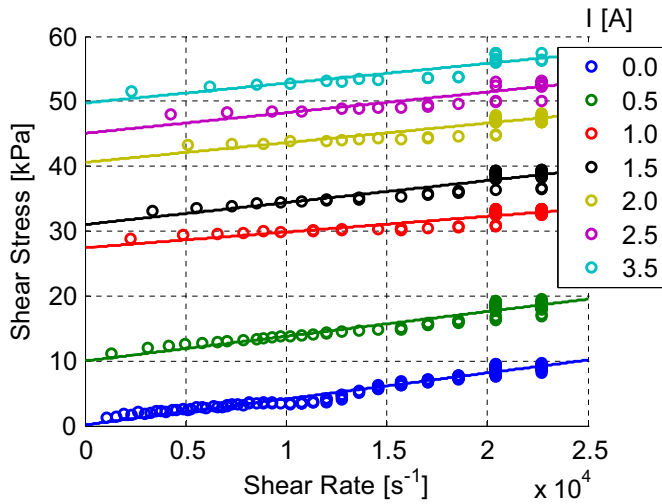


Fig. 9. Shear stress as a function of shear rate and applied current for MRF-140CG from the RVMREA, with Bingham plastic fit.

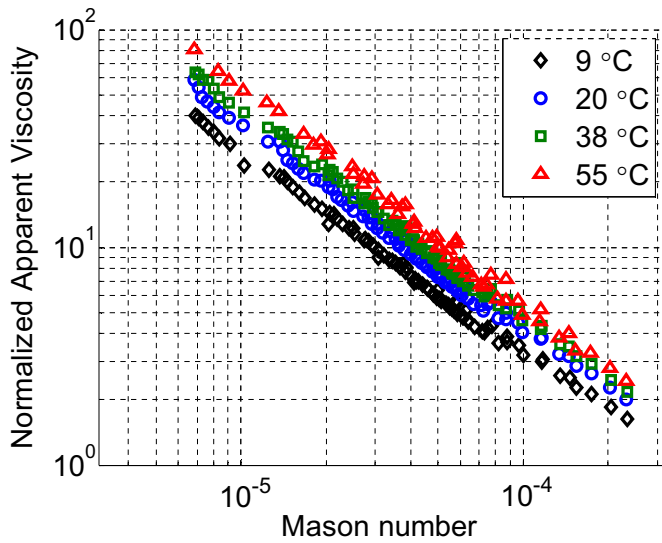


Fig. 10. Normalized apparent viscosity vs. Mason number without temperature correction, for MRF-132DG.

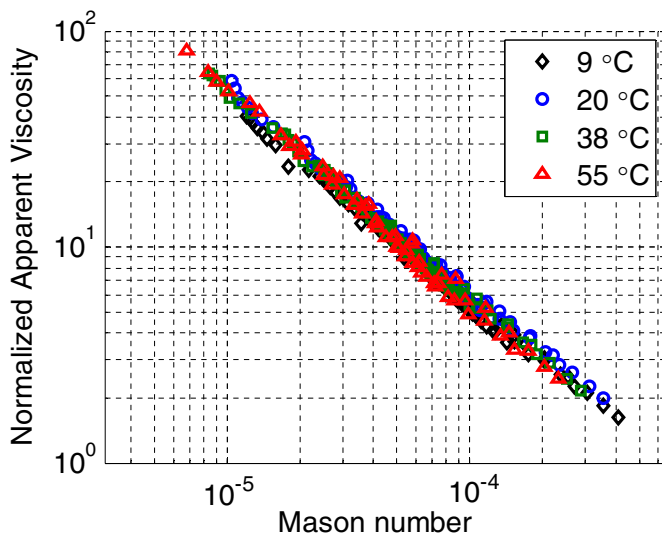


Fig. 11. Normalized apparent viscosity vs. Mason number incorporating the temperature correction, for MRF-132DG.

the carrier fluid viscosity. As one would expect, low-temperature tests exhibit a higher fluid viscosity and thus a higher viscous force component than high-temperature tests. Due to the fact that the Mason number is directly proportional to the viscosity, the temperature correction term from Eq. (9) accounts for this and effectively shifts the lower-temperature curves rightward. Fig. 11 shows the results of using the temperature-corrected Mason number given by Eq. (10). The data collapse to a single master curve, showing that temperature can now be presented along with shear rate, solids loading, and suspension magnetization to completely characterize the MR fluid performance across a wide range of shear rates. The carefully detailed experiments that provided the various data sets used in this series of analysis have become unnecessary, as a single master curve of normalized apparent viscosity versus Mason number can now be used to extrapolate to a wide array of operating conditions.

### 3.3. Comparison of Mason number at different device scales

Unlike the experiments using the Searle cell magnetorheometer instrument, the rotation testing of the rotary vane MREA was not performed with a controlled temperature environment. Each test was begun from room temperature, but from Fig. 9 it is clear that increased amounts of resistive and viscous heating occurred at higher applied currents. To minimize variations from this temperature difference, the first six seconds of experimental measurements can be used from each data set to yield a common, average temperature of approximately 55 °C.

The Mason number can be calculated for both the inner and outer gap regions, but since the shear rate and shear stress are dependent on the chosen radius, the two Mason number values are nearly identical; in all proceeding analysis, the inner gap region is used. Using the high shear rate, field off case to normalize apparent viscosity results across the entire data set, apparent viscosity trends with respect to the nondimensional Mason number shows that data for different shear rates and applied magnetization collapse to a single curve. Fig. 12 shows that the data in this study tends to agree with the results from previous research, although these experiments use MRF sheared in a concentric cylinder configuration and at rates approximately 25 × that used in the original work [9].

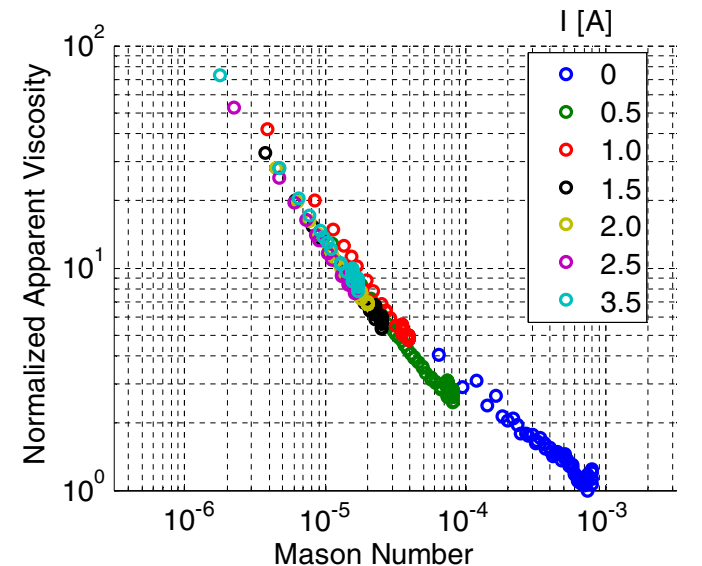


Fig. 12. Normalized apparent viscosity versus Mason number for the rotary vane MREA containing MRF-140CG up to  $\dot{\gamma} = 25,000 \text{ s}^{-1}$ .

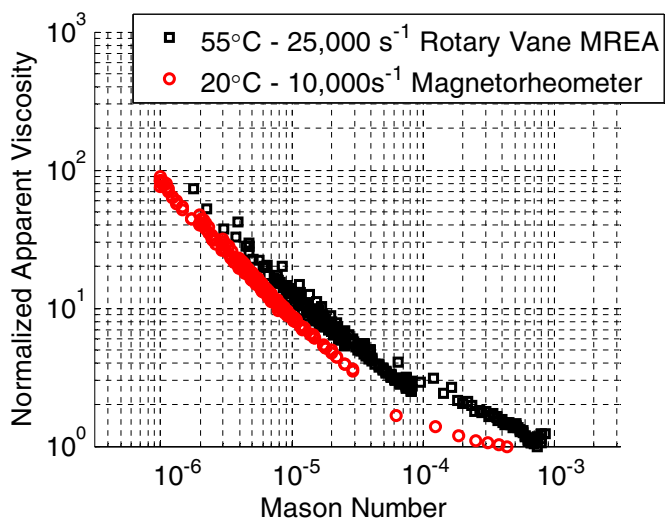


Fig. 13. Normalized apparent viscosity versus non-temperature corrected Mason number for the Searle magnetorheometer and the RVMREA containing MRF-140CG.

This nondimensionalized plot for the rotary vane MREA performance can now be directly compared with the results from the Searle cell magnetorheometer, even though these systems differ in maximum operating speed and system scale. Because the rotary vane MREA has an operating gap diameter nearly 10 × that of the Searle cell magnetorheometer, it can generate 15.5 ft-lbs of torque at shear rates up to 25,000 s<sup>-1</sup>, as compared to the Searle cell instrument’s 0.5 ft-lbs of torque at rates up to 10,000 s<sup>-1</sup>.

Fig. 13 shows the result of both nondimensionalized plots using Mason number for the full-scale rotary vane damper and the Searle cell magnetorheometer, each performed using the 40 vol% MR fluid manufactured by LORD Corporation, MRF-140CG. Note that while both curves exhibit the characteristic collapse within themselves, the two lines are not superimposed due to the temperature differences present during each characterization test. This can be ameliorated by using the temperature-corrected Mason number (Eq. (10)) to shift the curves by modifying the carrier fluid viscosity term appropriately. After doing this, Fig. 14 demonstrates that the two plots lie along the same master curve, indicating that the performance of these two different shear mode MR energy

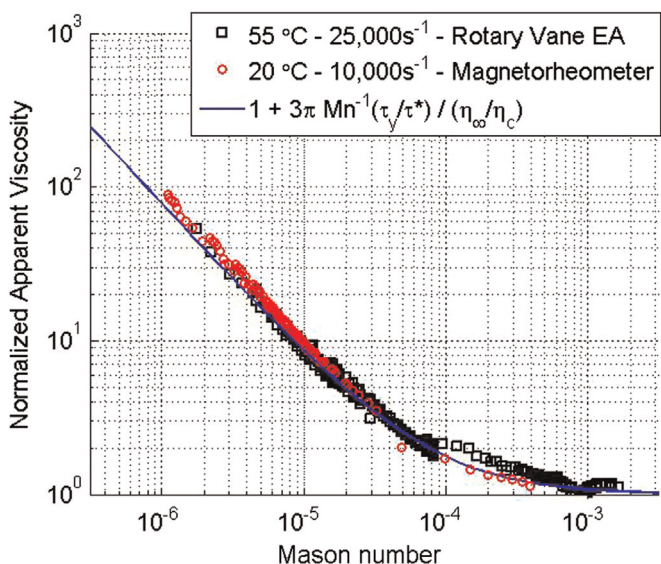


Fig. 14. Normalized apparent viscosity versus temperature corrected Mason number for the Searle magnetorheometer and the RVMREA containing MRF-140CG.

absorbers, operating at different shear rates, magnetic field strengths and temperatures can be described through the non-dimensional Mason number.

A curve can be fitted to this data using an equation of the following form [21]:

$$\eta_{app}/\eta_{\infty} = 1 + KMn^{-1} \tag{18}$$

Here  $K$  is a fit parameter that can be expressed in terms of two physically relevant nondimensional ratios, the normalized yield stress (yield stress over a reference interparticle stress),  $\tau_y/\tau^*$ , and the normalized plastic viscosity,  $\eta_{\infty}/\eta_c$ .  $K$  is sometimes referred to in the literature as a “critical Mason number”, and this can be extended to show that  $K$  varies linearly with the MR fluid volume fraction,  $\phi$ . Our analysis uses a modified form of Klingenberg’s Mason number, which contains a volume fraction term, and so this results in an expression of the well known result that yield stress varies linearly with volume fraction. In Fig. 14 the form used for  $K$  is given below, where the nondimensional ratio parameters are  $\eta_{\infty} = 0.59 \text{ Pa s}$  and  $\tau_y/\tau^* = 0.5$  [14].

$$K = 3\pi \frac{\tau_y/\tau^*}{\eta_{\infty}/\eta_c} \tag{19}$$

Therefore, if the fluid parameters used to determine  $K$  are known, either experimentally determined for novel MR formulations or provided by the manufacturer, the master curve can be calculated and a temperature correction factor can be used as a design benchmark for a family of scalable, shear mode devices.

#### 4. Conclusions

Rotary vane MREAs for shock impact operation at shear rates well over  $\dot{\gamma} = 25,000 \text{ s}^{-1}$  are currently designed using material properties measured at low shear rate, that is, for shear rates less than  $1000 \text{ s}^{-1}$ . This research examines a nondimensional Mason number analysis used to scale experimental data between different devices.

Incorporating a Reynolds temperature correction factor, data from both experiments is shown to collapse to a single master curve, supporting the use of Mason number to correlate low- and high-shear rate characterization data. This nondimensional analysis shows that the typical low shear rate data can be scaled to a practical device having over 78 times the active surface area, across a wide range of temperatures (9–55 °C) and operating speeds (up to  $\dot{\gamma} = 25,000 \text{ s}^{-1}$ ), such that performance can be predicted from only knowledge of the MR fluid properties. Plotting normalized apparent viscosity versus Mason number causes flow curve data to collapse at shear rates up to 25,000 s<sup>-1</sup>.

By accounting for temperature differences, the collapse of the curves can be improved drastically. The temperature corrected Mason number provides a simple and effective means of comparison between different shear rates, applied field strengths, and operating temperatures. Plots of apparent viscosity versus Mason number offer an alternative design metric, which is based solely on the properties of the chosen MRF and can be reliably scaled to devices of different size and operating speeds. Connecting laboratory experiments with practical applications using Mason number can expand the design space of MREAs to high velocity impacts.

#### Acknowledgment

This research was supported by the National Defense Science and Engineering Graduate Fellowship, 32 CFR 168a to A. Becnel,

and the Department of Aerospace Engineering at the University of Maryland.

## References

- [1] M. Mao, W. Hu, Y. Choi, N. Wereley, A magnetorheological damper with bifold valves for shock and vibration mitigation, *J. Intell. Mater. Syst. Struct.* 18 (12) (2007) 1227.
- [2] G. Hiemenz, W. Hu, N. Wereley, Semi-active magnetorheological helicopter crew seat suspension for vibration isolation, *J. Aircr.* 45 (3) (2008) 945–953.
- [3] G. Hiemenz, W. Hu, N. Wereley, Adaptive magnetorheological seat suspension for the expeditionary fighting vehicle, *J. Phys.: Conf. Ser.* 149 (1) (2009).
- [4] H. Sahin, X. Wang, F. Gordaninejad, Temperature dependence of magnetorheological materials, *J. Intell. Mater. Syst. Struct.* 20 (2009) 2215–2222.
- [5] D. Knezevic, V. Savic, Mathematical modeling of changing of dynamic viscosity, as a function of temperature and pressure, of mineral oils for hydraulic systems, *Facta Univ.: Mech. Eng.* 4 (1) (2006) 27–34.
- [6] A. Becnel, W. Hu, N. Wereley, Measurement of magnetorheological fluid properties at shear rates of up to 25,000 1/s, *IEEE Trans. Magn.* 48 (no. 11) (2012) 3525–3528.
- [7] M. Jolly, J. Bender, J. Carlson, Properties and applications of commercial magnetorheological fluids, *J. Intell. Mater. Syst. Struct.* 10 (1) (1999) 5–13.
- [8] R. Allan, S. Mason, Particle behaviour in shear and electric fields. I. Deformation and burst of fluid drops, *Proc. R. Soc. A* 267 (1328) (1962) 45–61.
- [9] D. Klingenberg, J. Ulicny, M. Golden, Mason numbers for magnetorheology, *J. Rheol.* 51 (5) (2007) 883–893.
- [10] J. Ginder, L. Davis, Shear stresses in magnetorheological fluids: role of magnetic saturation, *Appl. Phys. Lett.* 65 (26) (1994).
- [11] B. Kavlicoglu, F. Gordaninejad, X. Wang, A unified approach for flow analysis of magnetorheological fluids, *J. Appl. Mech.* 78 (4) (2011) 10.
- [12] O. Volkova, G. Bossis, M.B.V. Guyot, A. Reks, Magnetorheology of magnetic holes compared to magnetic particles, *J. Rheol.* 44 (1) (2000) 14.
- [13] B. de Gans, N. Duin, D. van den Ende, J. Mellema, The influence of particle size on the magnetorheological properties of an inverse ferrofluid, *J. Chem. Phys.* 113 (5) (2000) 11.
- [14] S. Sherman, A. Becnel, N. Wereley, Relating Mason number to Bingham number in magnetorheological fluids, *J. Magnetism and Magnetic Materials*, (2015), this issue.
- [15] W. Hu, G. Ngatu, G. Hiemenz, N. Wereley, J. Woodhouse, Lightweight magnetorheological energy attenuation system for rotorcraft seats, in: *American Helicopter Society Forum*, Fort Worth, TX, vol. 68, 2012.
- [16] P. Estelle, C. Lanos, A. Perrot, Processing the Couette viscometry data using a Bingham approximation in shear rate calculation, *J. Non-Newton. Fluid Mech.* 154 (1) (2008) 31–38.
- [17] H. Choi, I. Jang, J. Lee, S.B.A. Pich, H.-J. Adler, Magnetorheology of synthesized core-shell structured nanoparticle, *IEEE Trans. Magn.* 41 (10) (2005) 3448–3450.
- [18] F. Morrison, in: K. Gubbins (Ed.), *Understanding Rheology*, 1st ed., Oxford University Press, New York, 2001.
- [19] National Instruments, *LabVIEW Manual*, 2012. [Online]. Available: (<http://www.ni.com/pdf/manuals/320999e.pdf>). (accessed 27 08 13).
- [20] QuickSilver Controls, Inc., August 2011. [Online]. Available: ([www.qcontrol.com](http://www.qcontrol.com)).
- [21] L. Marshall, C.F. Zukoski, J.W. Goodwin, Effects of electric fields on the rheology of non-aqueous concentrated suspensions, *J. Chem. Soc. Faraday Trans. 1* (85) (1989) 2785–2795.